Article

Soil Salinity Assessing and Mapping Using Several Statistical and Distribution Techniques in Arid and Semi-Arid Ecosystems, Egypt

Mohamed E. Fadl [1], Mohamed E. M. Jalhoum [2], Mohamed A. E. AbdelRahman [3,*], Elsherbiny A. Ali [4], Wessam R. Zahra [5], Ahmed S. Abuzaid [5], Costanza Fiorentino [6], Paola D'Antonio [6], Abdelaziz A. Belal [2] and Antonio Scopa [6,*]

[1] Division of Scientific Training and Continuous Studies, National Authority for Remote Sensing and Space Sciences (NARSS), Cairo 11769, Egypt
[2] Division of Agricultural Applications, Soil and Marine Sciences, National Authority for Remote Sensing and Space Sciences (NARSS), Cairo 11769, Egypt
[3] Division of Environmental Studies and Land Use, National Authority for Remote Sensing and Space Sciences (NARSS), Cairo 11769, Egypt
[4] Geography Department, Faculty of Arts, Zagazig University, Zagazig 44519, Egypt
[5] Soils and Water Department, Faculty of Agriculture, Benha University, Benha 13518, Egypt
[6] Scuola di Scienze Agrarie, Forestali, Alimentari ed Ambientali (SAFE), Università degli Studi della Basilicata, Via dell'Ateneo Lucano, 10-85100 Potenza, Italy
[*] Correspondence: maekaoud@narss.sci.eg (M.A.E.A.); antonio.scopa@unibas.it (A.S.);
Tel.: +20-100-4781114 (M.A.E.A.); +39-(0)971-25240 (A.S.)

Abstract: Oasis lands in Egypt are commonly described as salty soils; therefore, waterlogging and higher soil salinity are major obstacles to sustainable agricultural development. This study aims to map and assess soil salinization at El-Farafra Oasis in the Egypt Western Desert based on salinity indices, Imaging Spectroscopy (IS), and statistical techniques. The regression model was developed to test the relationship between the electrical conductivity (EC_e) of 70 surface soil samples and seven salinity indices (SI 1, SI 2, SI 5, SI 6, SI 7, SI 8, and SI 9) to produce soil salinity maps depending on Landsat-8 (OLI) images. The investigations of soil salinization and salinity indices were validated in a studied area based on 30 soil samples; the obtained results represented that all salinity indices have shown satisfactory correlations between EC_e values for each soil sample site and salinity indices, except for the SI 5 index that present non-significant correlations with R^2 value of 0.2688. The SI 8 index shows a higher negative significant correlation with EC_e and an R^2 value of 0.6356. There is a significant positive correlation at the ($p < 0.01$) level between SI 9 and EC_e (r = 0.514), a non-significant correlation at the ($p < 0.05$) level between soil EC_e and SI 1 index (r = 0.495), and the best-verified salinity index was for SI 7 that has a low estimated RMSE error of 8.58. Finally, the highest standard error (R^2) was represented as EC_e (dS m^{-1}) with an R^2 of 0.881, and the lowest one was SI 9 with an R^2 of 0.428, according to Tukey's test analysis. Therefore, observing and investigating soil salinity are essential requirements for appropriate natural resource management plans in the future.

Keywords: soil salinity; statistical analyses; remote sensing; El-Farafra Oasis

1. Introduction

The problem of soil salinization is the most significant environmental issue in predominantly arid and semi-arid regions of Egypt, which are characterized by low rainfall rates, high temperature and evaporation values, and soil fertility that reduces seed growth, crop production, fertility, and agricultural ecological sustainability development. Wherefore, soil salinity monitoring, prediction, and mapping are necessary to alleviate land degradation in arid regions wherein massive data related to saline soils and their characteristics, distribution areas, and salinity process dynamics do not have to be obtained. Traditional irrigation

methods and poor drainage systems can be considered prevalent human-induced activities that lead to secondary soil salinization; therefore, monitoring and mapping soil salinity have become of great importance in overcoming this problem [1,2]. Soil salinity temporal and spatial variability information is required to minimize the adversarial effects of this important environmental problem on agricultural productivity [3]. Numerous salinity indices produced using satellite images and simple or complicated data combinations of spectral band ratios have been applied to recognize saline soil spatio-temporal distribution in several case studies. These indices generally achieve Visible Near-Infrared (vis-NIR) bands and are more related to multispectral images slightly or moderately high of relevant saline soils, comparatively higher than non-saline soils spectral reflectance in vis-NIR bands [4]. Moreover, extremely salt-affected soils show higher spectral responses compared to moderately or highly saline soils [5]. Multispectral sensors, such as the Landsat series, have delivered much potential for sequential, rapid, and low-cost observation, detection, and mapping of soil salinity [6,7]. Egyptian lands are suffering from increasing soil salinization due to many factors such as climate factors, groundwater resources, and sub-standard soil management; soil salinity may provide an advance of toxicity problems according to salinity concentration increasing in soil solution and the absorption of surplus amounts by crops [8].

Satellite images and RS techniques are suitable tools for temporal monitoring and mapping soil salinity coupled with field measurements. Soil salinity mapping has developed as an undemanding process performed by using GIS practices, which shows soil salinity spatial distributions and salinization environmental hazards. Additionally, to determine the ability of satellite images to accurately map and monitor salinization processes it is necessary to compare the spatial salinity data with field studies. For the last two decades, remotely sensed imagery has demonstrated its ability to monitor salinity changes effectively from surface characteristics in real-time and at various scales. Some previous studies have revealed that optical sensors, such as vis-NIR or Short-Wave Infra-Red (SWIR) spectral bands, are promising for the sensing and detection of soil surface salinity [8–12].

Different spatial indices, such as the Normalized Difference Salinity Index (NDSI) and the Brightness Index (BI), were executed to examine the resources used by these indices during soil salinity mapping in arid and semi-arid regions [13].

Unfortunately, traditional sampling soil laboratory analysis methods are expensive, time-consuming, laborious, and require many preparatory stages and large amounts of chemicals for the determination of the properties, which can be harmful to the environment [14,15]. Hence, routine laboratory analysis is restricted to only a few soil samples; therefore, there is a global need for a new approach to soil analysis, which is faster and cost-efficient [16,17]. Imaging Spectroscopy (IS) has proven to be a vital tool for spatially distributing soil properties and generating maps. Moreover, spectroscopy works in the vis-NIR and Short-Wave Infrared (SWIR) region, offering the possibility of mapping soil salinization [18]. The IS tool has been used to study and map spatially distributed soil characteristics, such as soil Electrical Conductivity (EC_e), which could be quantitatively assessed and mapped using advanced technology of regression models under laboratory conditions or using imaging sensors [19]. Over the past 35 years, soil spectroscopy has provided a promising capability for identifying vegetation, rocks, and minerals. As a modern technology proven to be highly efficient for estimating soil salinization, regression models are faster and cheaper than conventional methods. Additionally, these tools are environmentally friendly, non-destructive, reproducible, and repeatable in analytical methods. The regression models were applied under both field and laboratory conditions to calculate several soil characteristics without soil sample preparation [20]. Spectral reflectance ranging between 0.35 and 2.5 μm is more suitable for estimating the majority of soil salinization [21]. The integration of Imaging Spectroscopy and regression models for the accurate prediction of soil salinization has become a promising tool for saving time, cost, and effort. Multivariate algorithms that are commonly used in soil spectroscopy to capture soil variability (spectral variables at a wavelength range) include the Linear Regression

Model (LRM), which is used for the quantitative analysis of soil parameters prediction [22]. Root Mean Square Error (RMSE) was reported as a prediction error for soil salinization estimations and validation of that concentration from spectral data. The coefficients of multiple determinants, such as the correlation square (R^2) between the response and predicted values, were also unsuitably regression computed [23].

Geostatistical analysis is an effective method for studying, analyzing, and evaluating the spatial distribution of soil properties and their changes, and it has had a significant and effective contribution to reducing error rates and increasing production efficiency [9]. Ordinary Kriging (OK) model is a largely widespread technique used to predict the spatial distribution of soil properties.

The principal aim of this research paper is to predict and map soil salinity to enhance the national management strategy program by using seven different soil salinity indices derived from Landsat-8 (OLI) images integrated with electrical conductivity (EC_e) field measurements from the El-Farafra Oasis of the Egyptian Western Desert using statistical and distribution techniques. Whereas, decision-makers, farmers, land-use planners, and agricultural inspectors require updated, reliable, and accurate assessments of the investigated area's soil salinity, and the extensive spatial-temporal variation in the salinity of soil leads to difficult and costly monitoring, especially on a regional scale, is a determinant of the use of satellite imagery, which contributes to the significant capability for soil salinization detection, and systematically collects relevant information and consolidates large spatial data formats.

2. Materials and Methods

2.1. The Investigated Area

The total area of El-Farafra Oasis is about 980 km^2 of a geological depression, it is the second-biggest Oasis by size in the Western Desert of Egypt, and it has the smallest population. The Oasis is located between latitude 26°40′00″ and 27°30′15″ N and longitude 27°05′00″ and 28°50′17″ E, and it lies in the large desert of Western Egypt centered between El-Bahariya and El-Dakhla Oases, as shown in Figure 1. According to the geography and geo-formations, the El-Farafra Oasis has many underground water wells spread out over the surface of the land, many of which are artesian, and some wells are used in cultivated land for irrigation. The climate of the area is characterized as a hot desert and experiences long, dry, and very hot summers, cold winters, very low rainfall, and high evapotranspiration. The average temperatures in the hot months are normally between 13.8 and 47.8 °C, with a mean of 22.1 °C [24], as shown in Figure 2. The soil climate of this area contains a *Torric* soil moisture regime and a *Thermic* temperature regime [25].

2.2. Remote Sensing and GIS Procedures

To calculate the soil salinity indices and generate the soil salinity maps for the study area, the following data were used:

1. The Landsat-8 (OLI) satellite image data were radiometrically, geometrically, and atmospherically corrected using ENVI 5.1 software [26] to minimize the radiometric distortions and atmospheric perturbations caused by clouds, aerosols, and other atmospheric particles, respectively. These data were downloaded from the United States Geological Survey (USGS) website through Path, 178 and Row, 41 obtained on 8 December 2021.
2. Field electrical conductivity (EC_e dS m^{-1}) measurements were conducted in May–July 2021. The soil salinity maps were generated using ArcGIS 10.2.2 software [27].
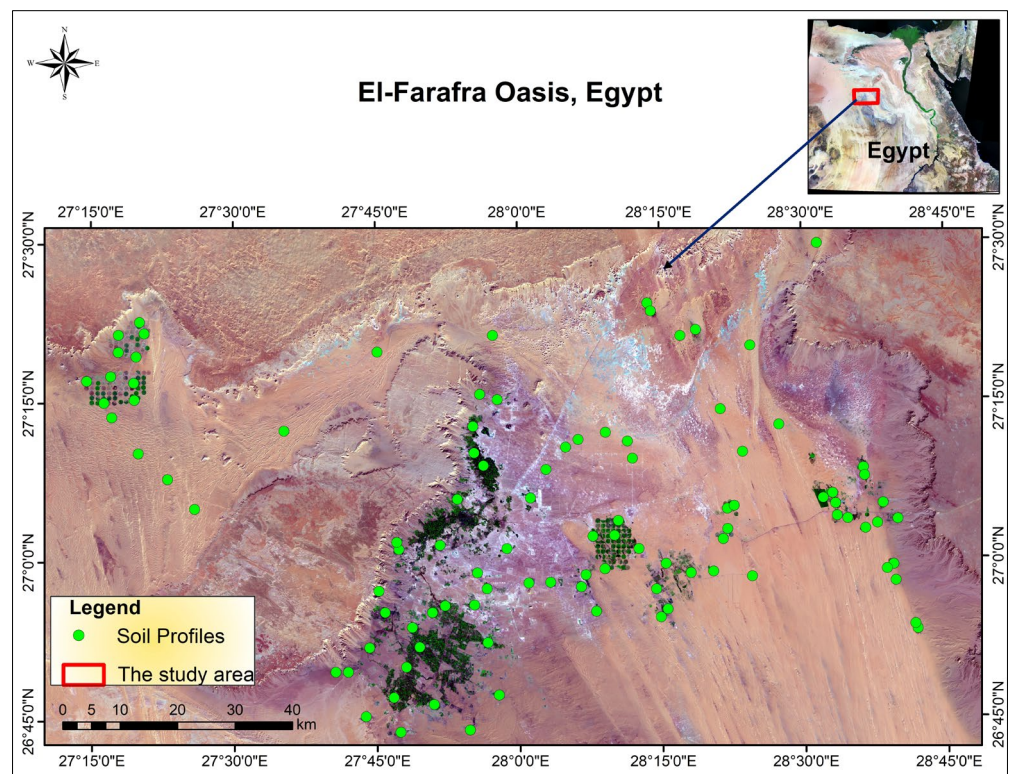
Figure 1. Soil profile location map in El-Farafra Oasis, (Landsat-8 (OLI) satellite image).
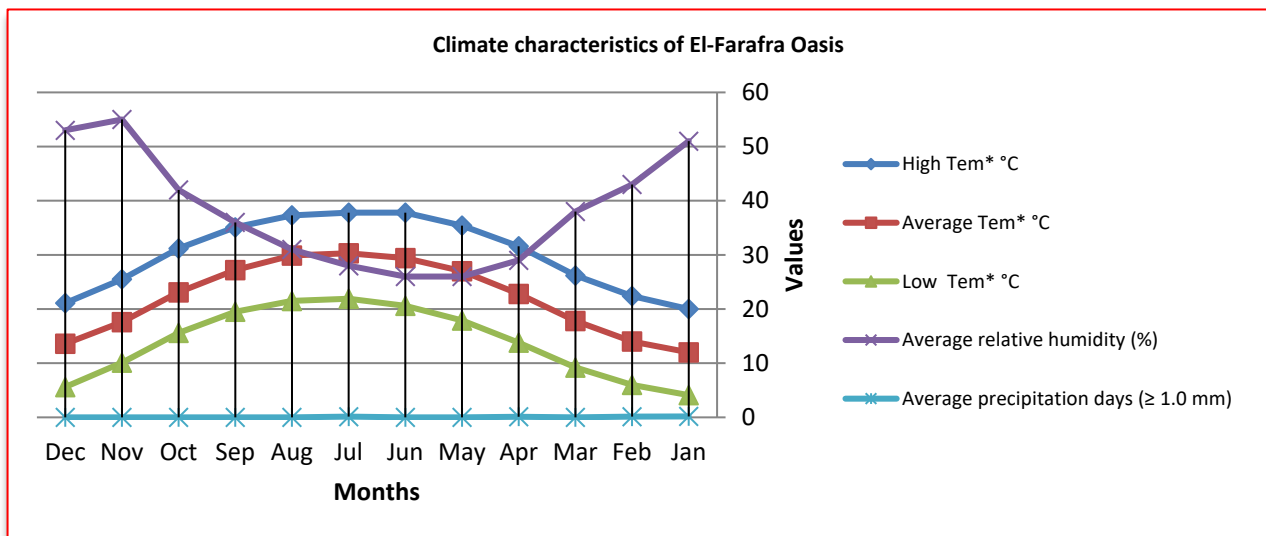

Figure 2. Climate characteristics of El-Farafra Oasis.

2.3. Field and Laboratory Work

The study area was represented by 100 surface soil samples with depths between 0 and 30 cm (where the highest salt accumulation is situated in the topsoil) that were collected to cover the spatial differences of the investigated area, then the soil's physical–chemical properties at each site were characterized according to the Soil Survey Staff [28]. The soil samples were air-dried and then passed through a 2 mm sieve. To investigate the soil salinization in the studied area, the soil salinity was determined through the use of electrical conductivity (EC_e) laboratory analyses, which were carried out in a saturated extract using a Beckman conductivity bridge at 25 °C, according to Bashour and Sayegh (2007) [29], and the soil samples were analyzed using standard methods for the Soil Survey

Staff [30]. Agronomic classification of soil salinity based on EC_e [31] was used to evaluate and classify soil salinization in the investigated area, which is characteristic at the genesis part (Table 1).

Table 1. Soil salinity classifications based on EC_e (dS m^{-1}) and effects on different crops.

Soil Salinity Classification	EC_e (dSm^{-1})	Crop Yieldaffected
Non-saline	0–2	Not affected, salinity effects are negligible
Slightly saline	2–4	Sensitive crops affected, yield loss for very sensitive crops
Saline	4–8	Many crops were affected, and their yields restricted
Strongly saline	8–16	Only tolerant crops bear this condition
Extremely saline	>16	A few very tolerant crops resist.

2.4. Soil Salinity Mapping

The soil salinity maps were generated from the Operational Land Imager (Landsat OLI-8) by using the base data related to the soil salinity indices in order to produce the maps that include five salinity classes (non-saline, slightly saline, moderately saline, highly saline, and extremely saline). Soil salinity was derived using the RS techniques developed through OLI-8 images, which are the most used RS data in soil salinity mapping. Soil salinity indices are mainly used to identify salt-affected soils based on the diverse reactions of salty soils to different Landsat-8 (OLI) image spectral bands. Table 2 shows the soil salinity indices used to generate the salinity maps for the investigated area; seven soil salinity indices, SI 1, SI 2, SI 5, SI 6, SI 7, SI 8, and SI 9, were functional and calculated to produce soil salinity maps depending on Landsat-8 (OLI) image bands of B2, B3, B4, and B5 (Red, Green, Blue, and Near-Infrared, respectively). The indices applying and calculating output images were necessary to produce soil salinity maps using GIS software due to the slicing approach level of diverse soil salinity indices range and map integration, and then the corresponding pixel values for each field sample locations were extracted to produce the relationship. The soil salinity classes were rated due to image bands pixel values to EC_e values of 2, 4, 8, 16, and more than 16 dS m^{-1}, and salinity degrees related to the observed values.

Table 2. Soil salinity indices description based on different spectrum band ratios of Landsat-8 (OLI).

Satellite Data	Soil Salinityindices	Band Ratios	Description	References
Landsat-8 (OLI)	SI 1	$SI\,1 = \sqrt{(B*R)}$	R =Band 4 = Red G = Band 3 = Green B = Band 2 = Blue NIR = Band 5 = Near Infra-Red	[32]
	SI 2	$SI\,2 = \sqrt{(G*R)}$		
	SI 5	$SI\,5 = \left(\frac{B}{R}\right)$		[33]
	SI 6	$SI\,6 = \frac{(B-R)}{(B+R)}$		
	SI 7	$SI\,7 = \frac{(G*R)}{(B)}$		
	SI 8	$SI\,8 = \frac{(B*R)}{(G)}$		[34]
	SI 9	$SI\,9 = \frac{(NIR*R)}{(G)}$		

2.5. Spatial Distribution Mapping (Geostatistical Workflow)

Geostatistics is a statistical class used to examine and predict the rates related to spatio–temporal features. Mapping and geostatistical techniques, such as semi-variogram γ (h),

cross-validation, kriging analyses, and kriged spatial distribution mapping appreciations, were used to calculate and create surface maps of variance structure for soil salinity. The semi-variogram experimental is the mean square graphical representation of variability between two distance nearest neighbors (h), as shown in the following equation [35]:

$$\gamma(h) = \frac{1}{2N(h)} \sum_{i=1}^{N(h)} [z(x_i + h) - z(x_i)]2$$

where γ (h) is the semi-variogram expressed as a magnitude function separation vector h, N (h) is the number of the examination pair's discrete points by distance h, and z (x_i) is the random variable at location x_i.

2.6. Developed Linear Regression Model

Linear regression test analysis was performed to authenticate the relationship between the field data EC_e values used as a dependent relative variable and the soil salinity indices, which were derived from satellite images as an independent variable. EC_e values were estimated for unmeasured locations by using the known salinity index values of the same location based on the generated plots [36]. A correlation coefficient test was computed to verify the relationship between the grounds EC_e values and the soil salinity indices extracted values; all of the statistical analyses were performed using the Microsoft Excel package and SPSS software.

2.6.1. Pearson Correlation Coefficient Analysis

The Pearson correlation coefficient is used to measure two variables (x and y) linear association strength, where the value of (r = 1) means a perfect positive correlation and the value of (r = −1) means a perfect negative correlation, and where a value of (0) indicates no linear correlation [37]. The sample correlation coefficient between the two variables of x and y is denoted as r or rxy and can be computed as follows:

$$r_{xy} = \frac{cov(x, y)}{\sqrt{var(x)}\sqrt{var(y)}}$$

where cov(x, y) is the sample covariance of x and y, var(x) is the sample variance of (x), and var(y) is the sample variance of (y).

2.6.2. Root Mean Square Error (RMSE)

The RMSE error is the standard deviation of the prediction errors (residuals) that are computed to show whether the point data are far or concentrated around the best regression line. RMSE was used in the regression examination to confirm the experimental results and test the validity of the soil salinity indices; RMSE was calculated using the following equation [38]:

$$RMSE = \sqrt{1/N \sum_{i=1}^{n} (y - x)^2}$$

where N is the number of observations values, y represents the forecasted or expected values (unknown results), and x represents the observed values extracted from field data (known results).

2.6.3. Tukey's Range, Significant and Difference Test (Model Validation)

Tukey's range test, also known as the Tukey's HSD (honestly significant difference) test, is a single-step multiple comparison procedure and statistical test used to obtain the means (expected normal values and observed values) that are significantly different and detect any differences between these means greater than the expected standard error (R^2). Tukey's test compares the means of every treatment to the means of every other treatment; that is, it is applied simultaneously to the set of all pairwise comparisons and identifies any

difference between two means that is greater than the expected standard error [39]. Tukey's test is based on a formula very similar to that of the t-test. In fact, Tukey's test is essentially a t-test, except that it corrects for family-wise error rate. Tukey's test formula is as follows:

$$q_s = \frac{Y_A - Y_B}{SE} \tag{1}$$

where YA is the largest of the compared means, YB is the smallest of the compared means, and SE is the standard error of the summation means. The qs value can be compared to the q value extracted from the studied distribution values. If the qs value is larger than the critical value of q obtained from the distribution, the two means will be significantly different at the α: $0 \le \alpha \le 1$ level [40].

3. Results

3.1. Estimation of Soil Salinity Based on Landsat-8 (OLI) Data and Soil Salinity Indices

After calculating each soil salinity index (SI 1, SI 2, SI 5, SI 6, SI 7, SI 8, and SI 9) from the satellite images, pixel values with various ranges in all image bands were extracted, and then the corresponding EC_e values were compared with their exacted pixel values of the same location. Figure 3 represents the soil salinity spatial distribution in the investigated area, displaying the soil characteristics and trend extent of soil salinization processes, also representing total salinity and salinity classes.

The relationship between the appointed measured EC_e values and salinity index values derived from digital satellite images is required to generate soil salinity maps and evaluate soil salinity classes and rates. The soil samples were then averaged to provide a single spectrum for each target. Figure 4 shows the field-derived salt-affected average soil spectra that have relatively sparse canopies compared to the soil samples and, consequently, have significant reflectance across the visible, NIR, and SWIR spectra.

3.2. Devolved Linear Regression Model

As shown in Table 3 and Figure 5, the soil salinity values (EC_e), seven salinity indices (including SI 1, SI 2, SI 5, SI 6, SI 7, SI 8, and SI 9), and descriptive statistics that were generated from Landsat-8 (OLI) images with satisfactory correlations were distinguished between the salinity measured (EC_e) for each soil sample site and the salinity indices. However, the SI 5 index showed lower correlations with the EC_e readings, with a coefficient R^2 value of 0.2688, while the SI 8 index represents negative correlations with the EC_e readings, with an R^2 value of 0.6356. The linear regression results for seven different salinity indices of the year 2021 are illustrated in Table 4.

Table 3. Descriptive statistics of soil salinity indices and soil EC_e.

	Descriptive Statistics				
ID	Number of Soil Samples	Minimum	Maximum	Mean	Std. Deviation
EC_e (dS m^{-1})	100	1.20	39.60	11.53	9.40
SI 1	100	2.74	14.35	7.84	2.98
SI 2	100	2.58	15.77	8.26	3.40
SI 5	100	0.71	2.29	1.07	0.43
SI 6	100	−0.17	0.39	0.00	0.16
SI 7	100	1.60	19.53	9.2	4.77
SI 8	100	2.05	13.39	7.42	2.97
SI 9	100	4.53	12.89	7.76	2.24

(**A**)

(**B**)

(**C**)

Figure 3. *Cont.*

(**D**)

(**E**)

(**F**)

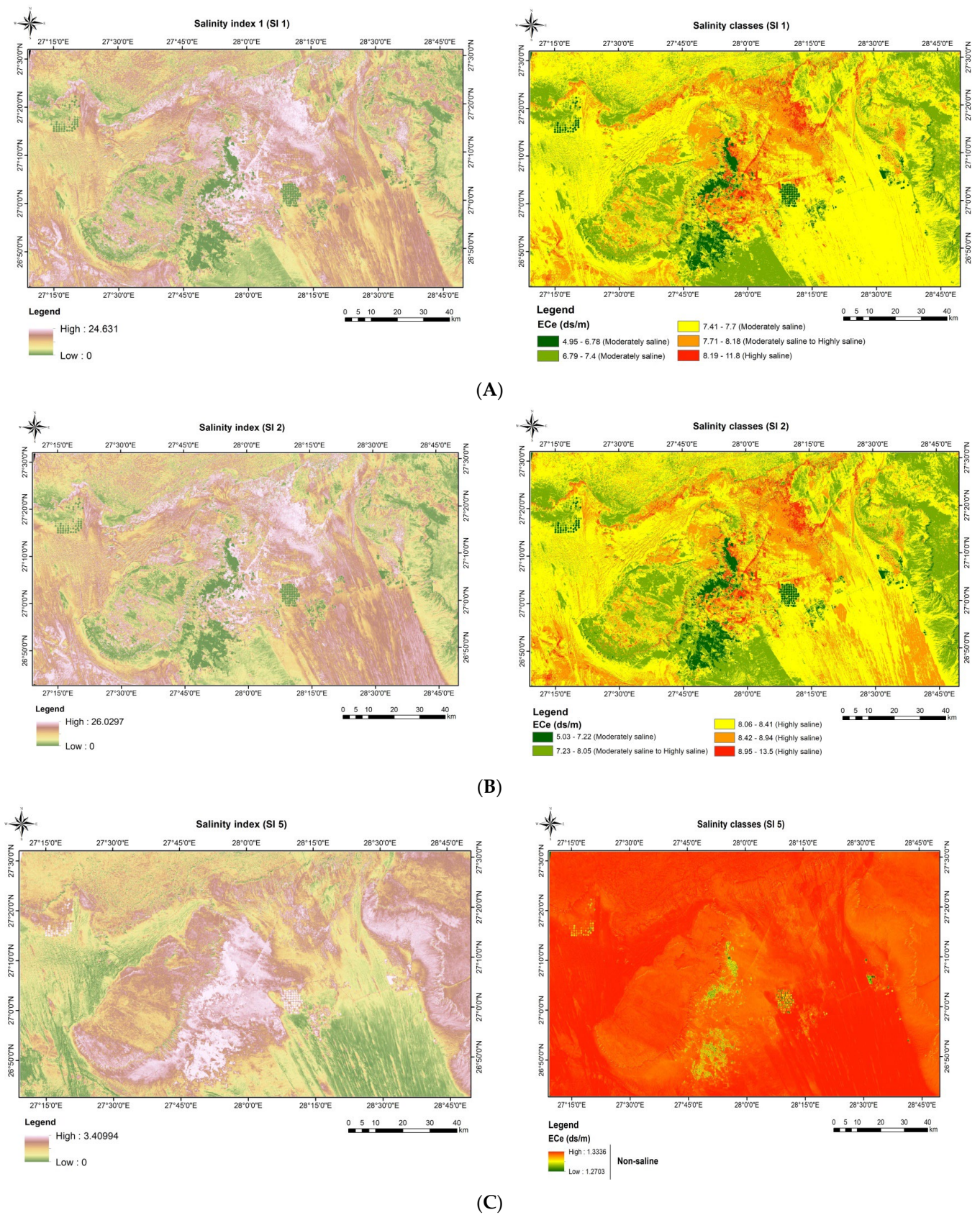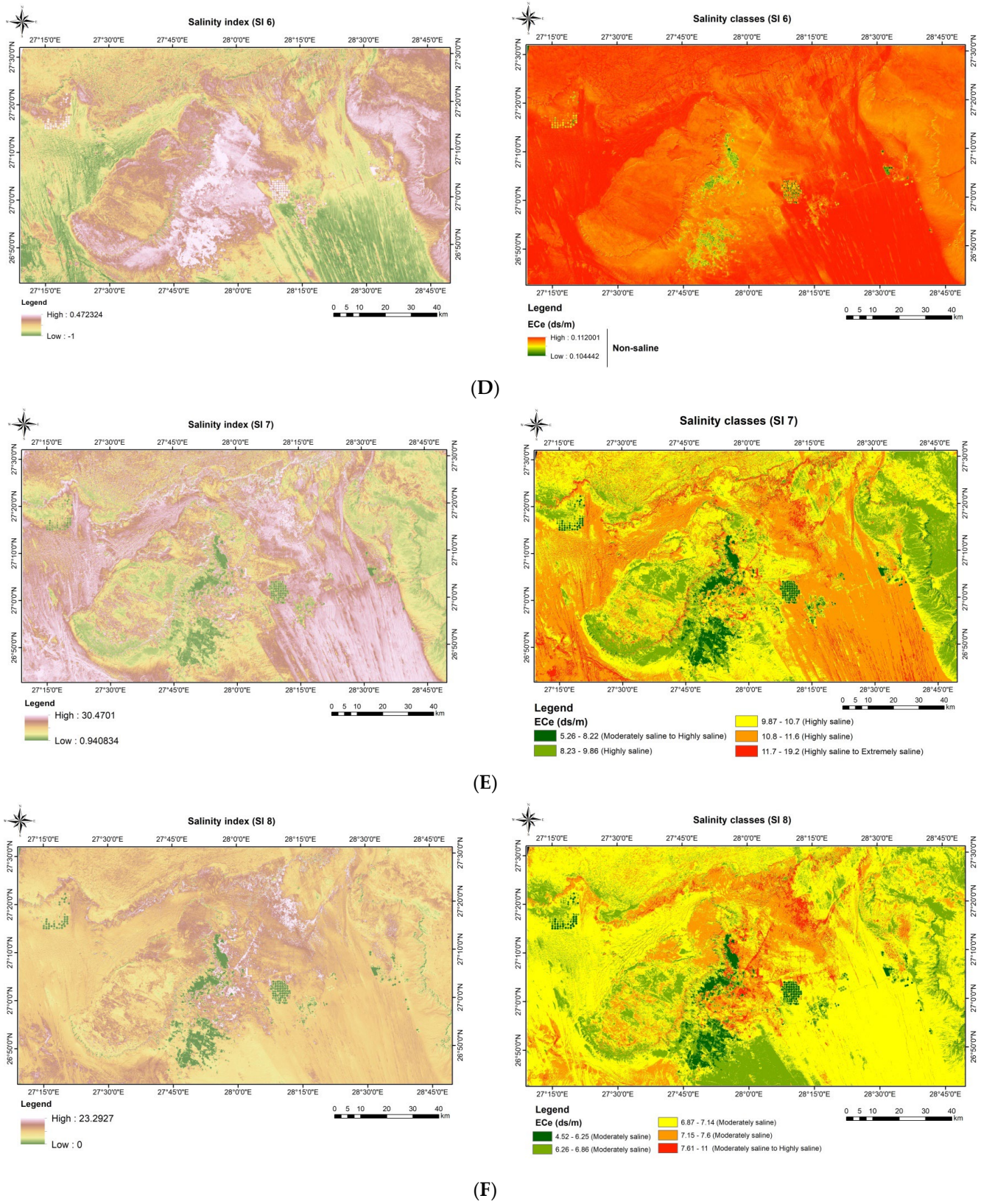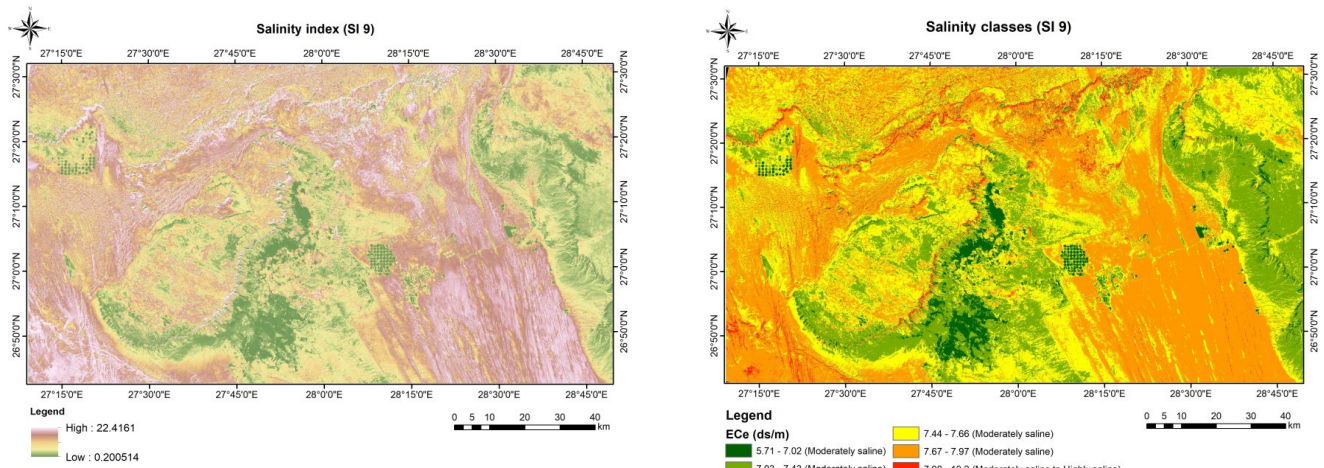**Figure 3.** *Cont.*

Figure 3. Soil salinity maps of the study area produced from salinity indices derived from Landsat-8 (OLI) spectral bands: (**A**) = SI 1; (**B**) = SI 2; (**C**) = SI 5; (**D**) = SI 6; (**E**) = SI 7; (**F**) = SI 8 and (**G**) = SI 9.
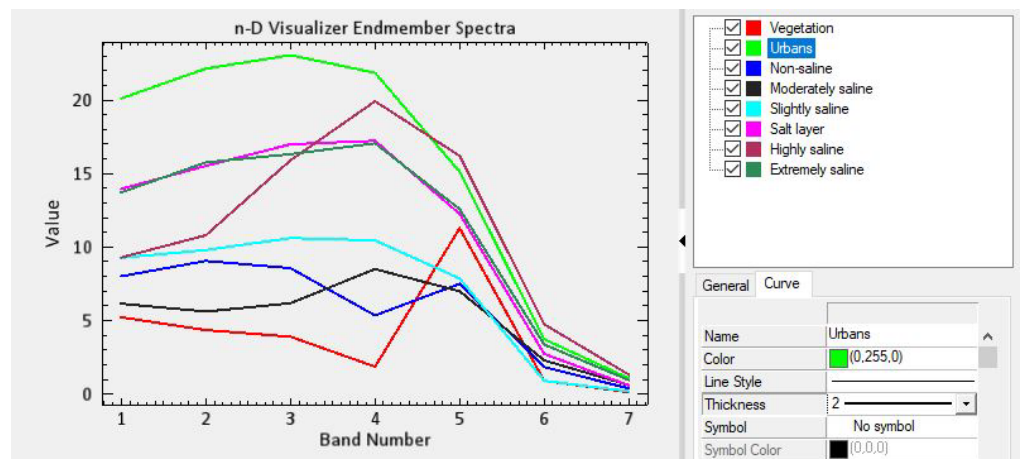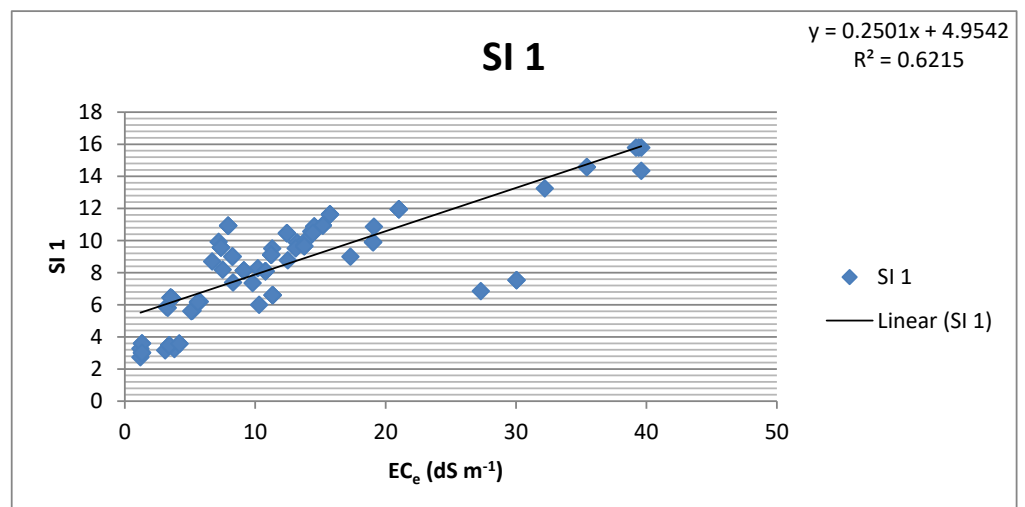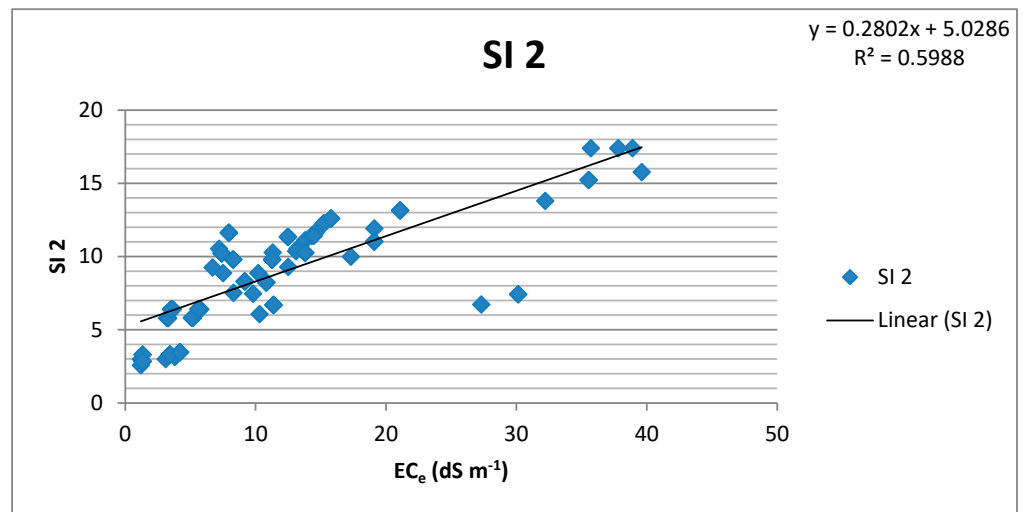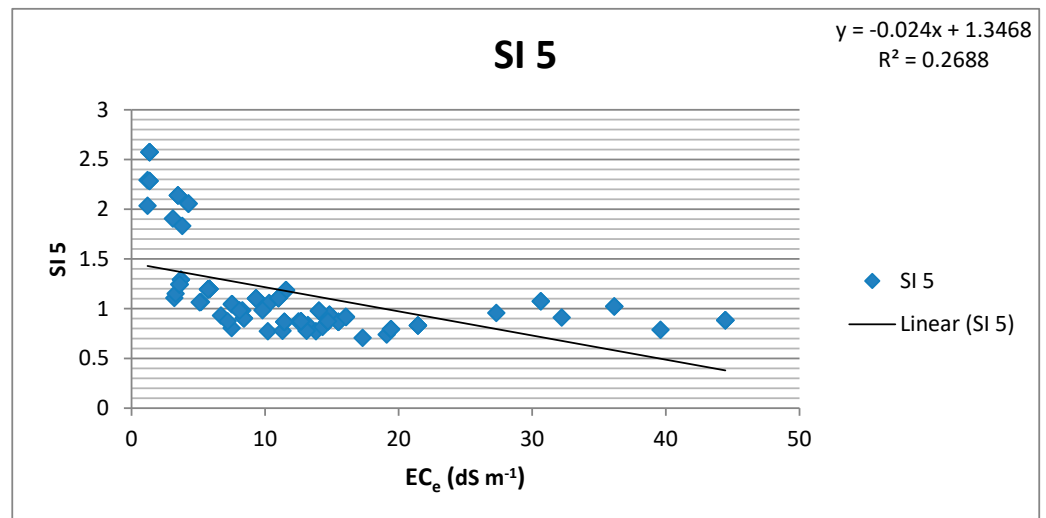

Figure 4. Field-derived salt-affected soils average spectra.

Figure 5. *Cont*.

(**B**)

(**C**)
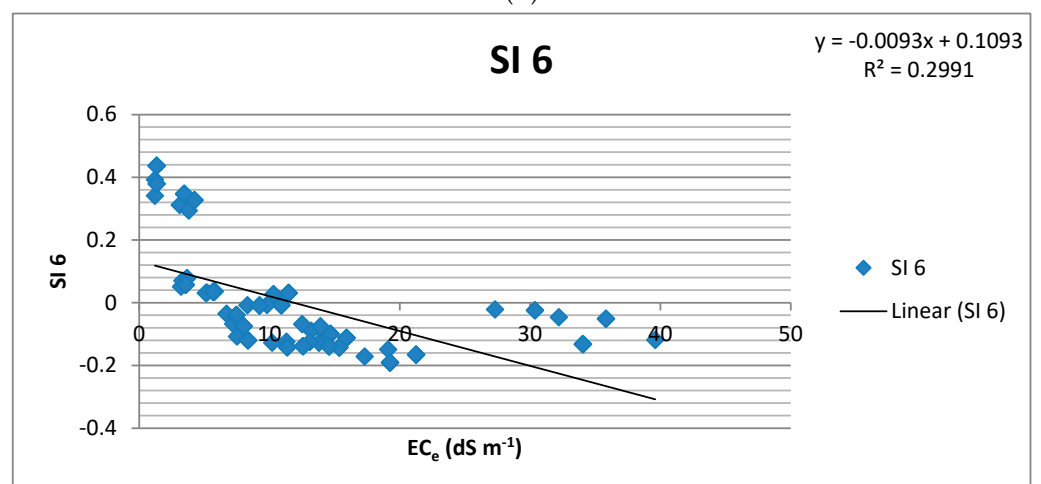
(**D**)

Figure 5. *Cont.*

(**E**)

(**F**)

(**G**)

Figure 5. Linear regression equations and coefficients of determination between laboratory soil salinity (EC$_e$) and soil salinity indices (SI$_S$): (**A**) = SI 1; (**B**) = SI 2; (**C**) = SI 5; (**D**) = SI 6; (**E**) = SI 7; (**F**) = SI 8 and (**G**) = SI 9.

Table 4. Linear regression results for seven different salinity indices of year 2021.

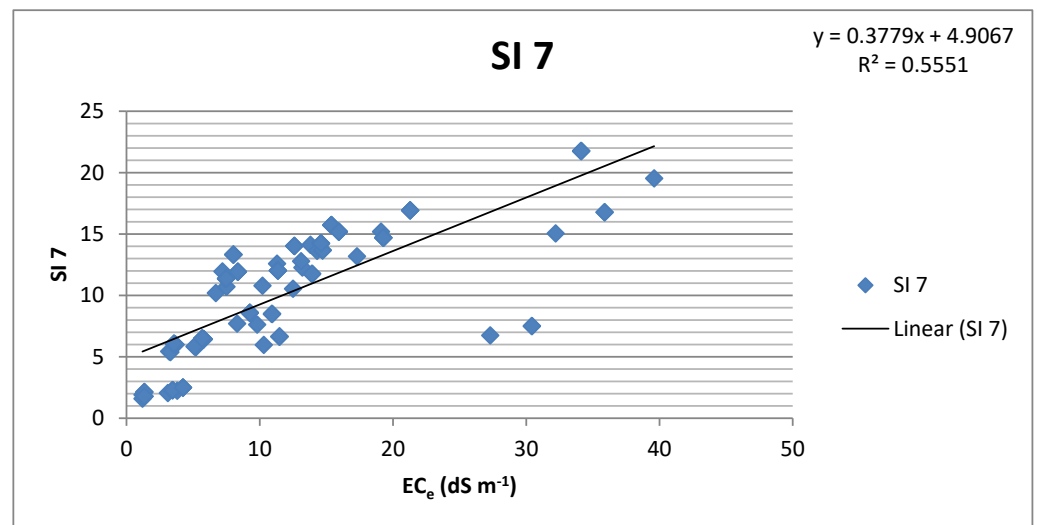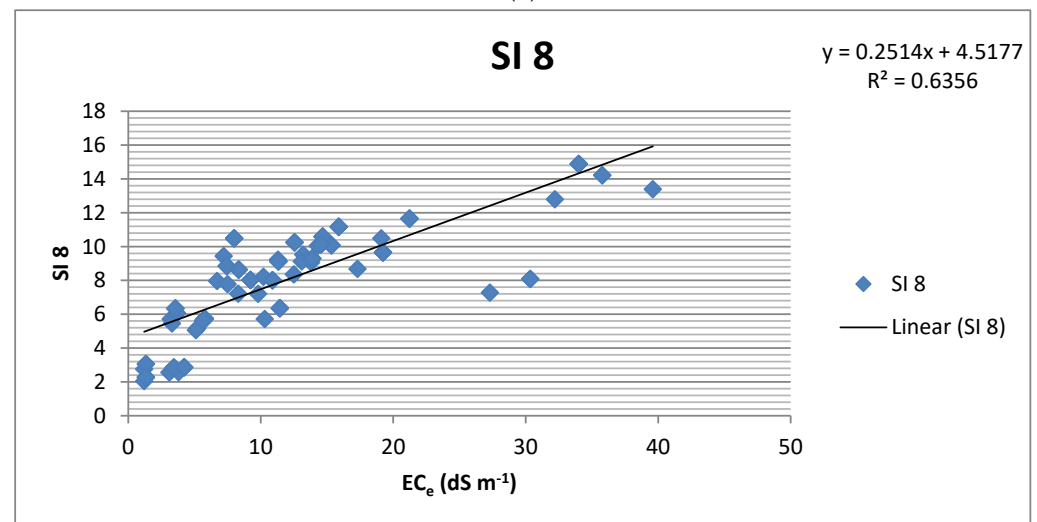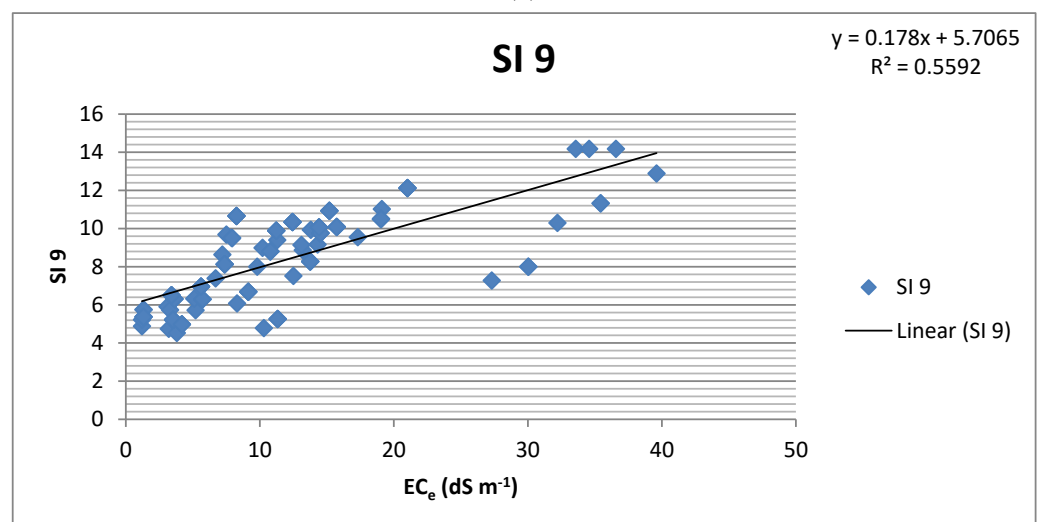| Salinity Index	Index Range	Index Rangereference	Date of Satellite Image	Number of Samples	R^2
SI 1	0–1				0.6215
SI 2					0.5988
SI 5	0–1.73				0.2688
SI 6		[1]	8-December-2021	100	0.2991
SI 7	0–1.42				0.5551
SI 8					0.6356
SI 9					0.5592

3.3. Pearson Correlation Coefficient Analysis

A Pearson correlation analysis was applied to understand the correlation between the soil EC_e and the soil salinity indices, then least-square linear regression analysis was conducted at the confidence level of the soil EC_e measurements in 2021. The correlation matrix among soil salinity indices and soil EC_e results are shown in Table 5 and Figure 6. The results indicated that there was a significant positive correlation at the $p < 0.01$ level between the soil EC_e and SI 9 index (r = 0.514), and there was a non-significant correlation at the $p < 0.05$ level between soil EC_e and (SI 1, SI 2, SI 7, and SI 8) indices (r = 0.495, 0.491, 0.479, and 0.492), respectively.

Table 5. Correlation matrix among soil salinity indices and soil EC_e.

	Pearson Correlations							
	EC_e (dS m^{-1})	SI 1	SI 2	SI 5	SI 6	SI 7	SI 8	SI 9
EC_e (dS m^{-1})	1							
SI 1	0.495 *	1						
SI 2	0.491 *	0.998 **	1					
SI 5	−0.308	−0.799	−0.801	1				
SI 6	−0.333	−0.833	−0.842	0.988 **	1			
SI 7	0.479 *	0.980 **	0.991 **	−0.808	−0.862	1		
SI 8	0.492 *	0.996 **	0.990 **	−0.826	−0.857	0.971 **	1	
SI 9	0.514 **	0.907 **	0.921 **	−0.686	−0.761	0.943 **	0.897 **	1

*. Correlation is significant at $p < 0.05$ level (2-tailed). **. Correlation is significant at $p < 0.01$ level (2-tailed).

3.4. Soil Salinity Values Prediction and Assessing Using Root Mean Square Error (RMSE)

The linear regression equations distinguished between the salinity measured in the laboratory for each soil sample and the salinity indices (SI 1, SI 2, SI 5, SI 6, SI 7, SI 8, and SI 9) have satisfactory correlations; i.e., y = 0.2501x + 4.9542; y = 0.2802x + 5.0286; y = −0.024x + 1.3468; y = −0.0093x + 0.1093; y = 0.3779x + 4.9067; y = 0.2514x + 4.5177; and y = 0.178x + 5.7065. Each soil salinity indices, respectively, were used to calculate the corresponding salinity index (x) values, for EC_e measurements of 2, 4, 8, and 16 dS m^{-1}, by inserting these values (y) in the equation. The calculated (x) values were then used to predict the EC_e salinity values for the study area, as shown in Table 6; then by using 70 soil samples, the efficiency of the soil salinity generated values was evaluated and assessed by estimated RMSE to verify the test efficiency depending on the degree of agreement between the observed and expected values, the obtained results indicated that the best-verified salinity index is SI 7 that has low estimated RMSE error of 8.58.
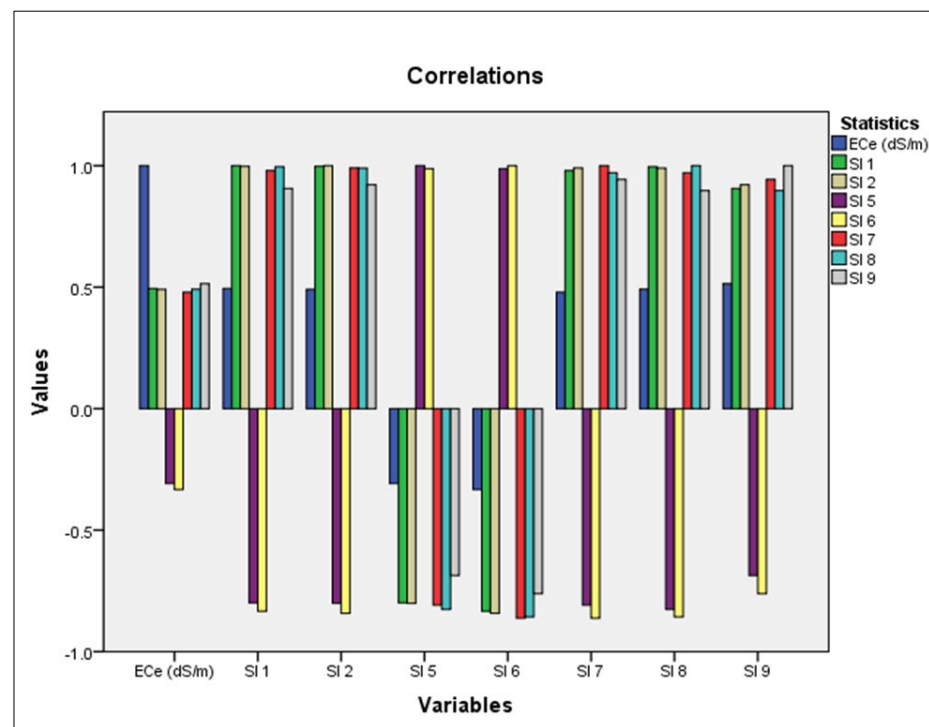
Figure 6. Pearson correlation among soil salinity indices and soil EC_e.

3.5. Tukey's Range, Significant and Difference Analysis (Model Validation)

Tukey's test was used to obtain the means (expected normal values and observed values of EC_e (dS m^{-1}) and accepted soil salinity indices (SI 1, SI 2, SI 7, SI 8, and SI 9) that have significant negative or positive correlations between those that have significantly different or detect any differences greater than the expected means standard error (R^2). For the examination of the linear regression model validation, 30 similar soil sample points, including the samples from each category of the five (5) soil salinity classes, were examined, and the output results for all of the indices of the satellite data and EC_e values revealed almost similar standard error (R^2) values ranging from 0.881 to 0.428, as shown in Figure 7A–F. The total estimated distribution parameters between the observed and expected means for EC_e and soil salinity indices are shown in Table 7.
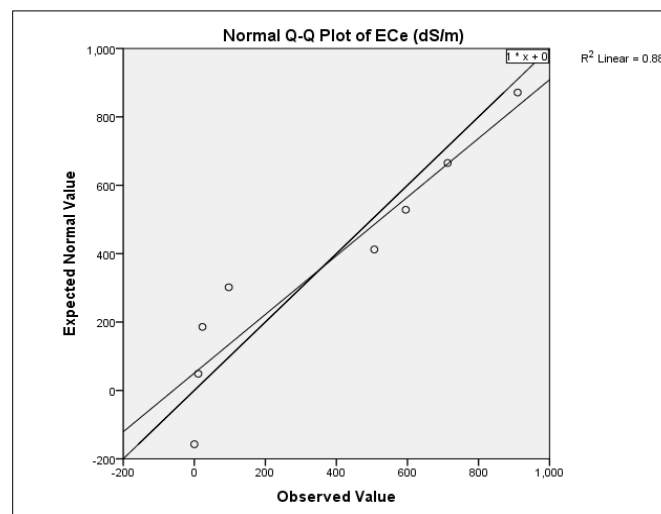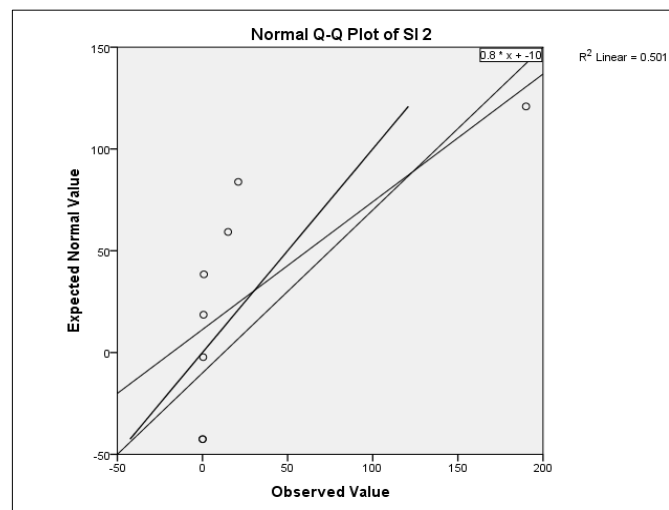

(A)

Figure 7. *Cont.*
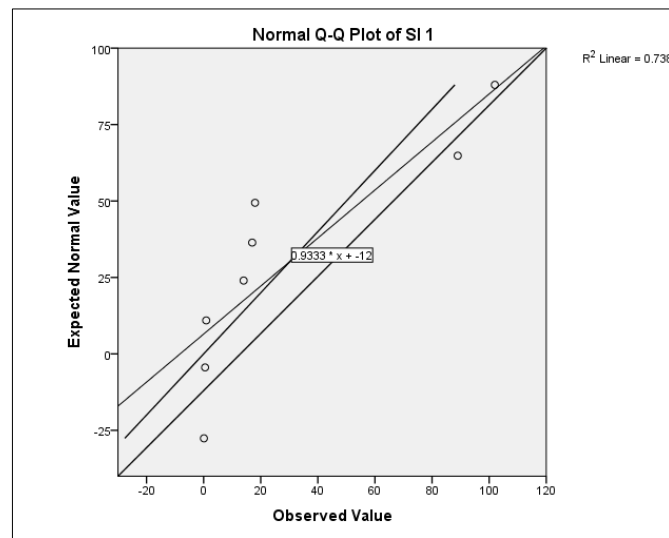
(**B**)

(**C**)
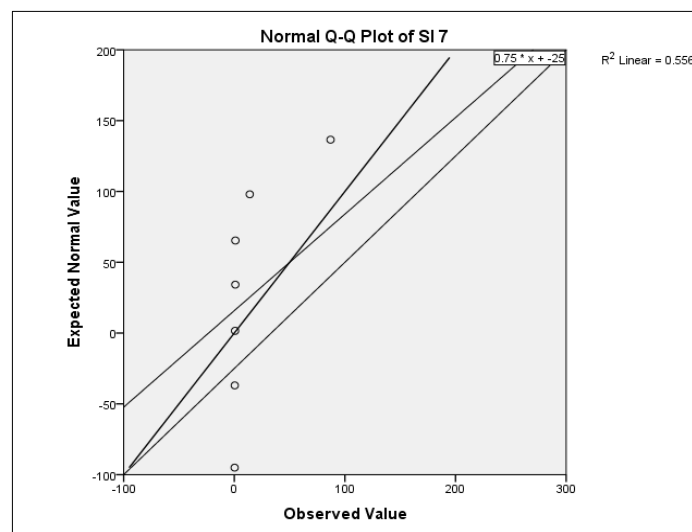
(**D**)

Figure 7. *Cont.*
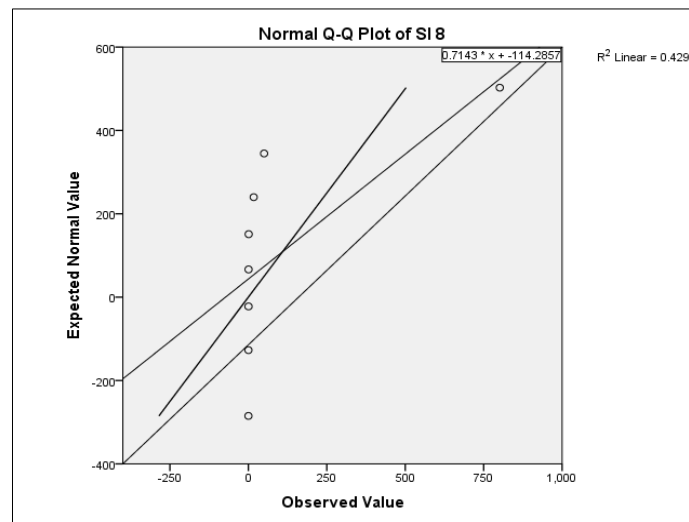
(**E**)
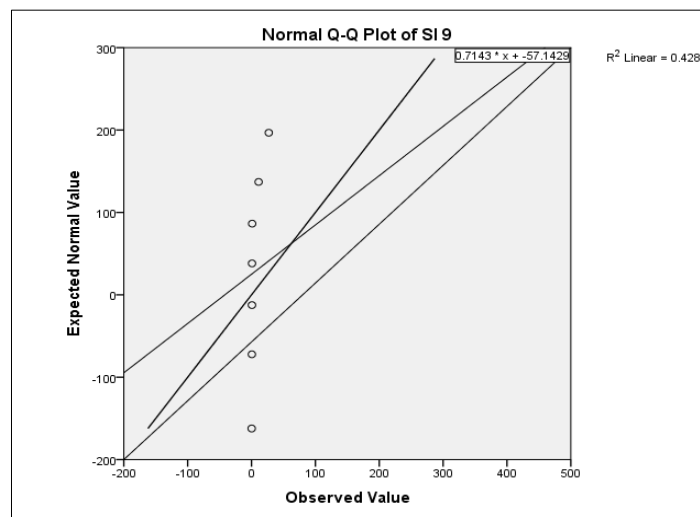
(**F**)

Figure 7. Normal Q–Q plot of soil salinity and soil salinity indices: (**A**) = EC_e (dSm^{-1}); (**B**) = SI 1; (**C**) = SI2; (**D**) = SI 7; (**E**) = SI 8 and (**F**) = SI 9.

Table 6. Soil salinity values prediction and assessment.

	Predict EC_e (dS m^{-1}) Salinity Values						
	SI 1	**SI 2**	**SI 5**	**SI 6**	**SI 7**	**SI 8**	**SI 9**
Minimum	5.64	5.75	1.29	0.11	5.51	5.03	6.51
Maximum	8.54	9.45	1.33	0.11	12.29	7.88	8.00
Mean	5.64	5.75	1.29	0.11	5.51	5.03	6.51
Std. deviation	0.75	0.95	0.01	0.00	1.80	0.75	0.40
Number of soil samples	70	70	70	70	70	70	70
RMSE	9.81	9.49	13.75	14.68	8.58	10.07	9.98

Table 7. Total estimated distribution parameters between observed means and expected means for EC_e and soil salinity indices.

		Estimated Distribution Parameters					
		EC_e (dS m^{-1})	SI 1	SI 2	SI 7	SI 8	SI 9
Normal Distribution	Observed mean	8.123	8.215	9.443	2.121	9.502	11.288
	Expected mean	9.735	1.946	3.040	1.110	3.246	4.598

4. Discussion

4.1. Estimation of Soil Salinization

Soil salinity refers to soil salt content, and salinization is a process of salt accumulation in soil. Salinity can give rise to natural processes, while soil salinization materializes through synthetic and natural processes, i.e., irrigation and salt tracks in the earth [41]. Soil salinity maps were generated depending on the OLI-8 image data and soil salinity indices to identify salt-affected soils based on the reactions of salty soils to different satellite image spectral bands (visible, NIR, and SWIR spectra). The results showed that by applying each soil salinity index, various ranges in all image bands were extracted, the corresponding EC_e values were compared with the exact pixel value of the same location, and then the soil salinity classes were rated in relation to the image band pixel values of the EC_e values of 2, 4, 8, and 16 dS m^{-1}. Furthermore, the degree of salinity was related to the observed values, which were then used to produce soil salinity maps using GIS software based on the range of the slicing approach level of diverse soil salinity indices and map integration. Therefore, Landsat-8 (OLI) images are a better method to produce soil salinity spatially distributed maps but require further investigative studies of such dependencies.

The method developed and used in this paper depends on image data and soil salinity indices based on a regression model can be used for other satellite data, such as those provided by Sentinel 1 and 2, and can be applied in other arid and semi-arid environments, these results are similar to those in the literature data [42]. Several studies have proved that the prediction of high soil salinity levels shows several non-linear relationships between the ground data (EC_e values) measured in the field and soil salinity indices' reflectance spectra [43].

4.2. Devolved Linear Regression Model

Linear regression tests analyze the relationship between two variables modeled through the appropriateness of a linear equation of the observed data. This test was performed to authenticate the relationship between the EC_e values and soil data from the satellite. The data in Tables 4 and 5 show that all of the salinity indices with satisfactory correlations were distinguished between EC_e values and the soil from the satellite, the SI 5 index showed lower correlations with the EC_e ($R^2 = 0.2688$), and the SI 8 index exhibited higher positive correlations ($R^2 = 0.6356$). These results are consistent with another study conducted in the Yellow River Delta situated on the northeast coast of China [44]; soil salinity was detected by means of a Moderate Resolution Imaging Spectroradiometer (MODIS) and by utilizing some soil salinity indices. The relationship between the EC_e values and soil reflectance spectra was investigated using the linear regression method [45].

Through the use of multiple regression techniques to estimate soil salinity in China, where several RS techniques, such as band math, have been conducted to develop uncorrelated factors of satellite image bands, the results represented that soil salinity indices data with EC_e measurements by applying multiple regression techniques showed comparatively accurate predictions [46].

4.3. Pearson Correlation Coefficient Analysis

The Pearson correlation coefficient is a statistical test used to statistically measure the relationships between some variables and the association between variables of interest

depending on the covariance method and was applied to understand the correlation between the soil EC_e and different soil salinity indices. The results indicated that there was a significant positive correlation at the $p < 0.01$ level between soil EC_e and the SI 9 index, and there was a non-significant correlation at the $p < 0.05$ level between soil EC_e and (SI 1, SI 2, SI 7, and SI 8) indices. This correlation is according to increasing and decreasing soil salinity ranges; therefore, these changes in salinity levels might be due to soil layer salt concentration, which refers to different modes of geological sedimentation due to the effects of different eras and human activities, respectively. Hammam and Mohamed, 2020 [47], used Pearson correlation coefficient analysis in their paper and represented that there are correlations between NDVI values, soil salinity, and the percentage of total toxic salts, where negative correlations were distinguished between NDVI and EC_e.

4.4. Soil Salinity Assessing Using Root Mean Square Error (RMSE)

The RMSE error is the standard deviation of prediction errors that are computed to show how far or concentrated the data are around the best regression line and is used in regression examination to confirm experimental results and test the validity of soil salinity indices [48]. The results in Table 6 indicate that the efficiency of soil salinity values generated by using 70 soil samples was evaluated and assessed by estimated RMSE to verify test efficiency depending on the degree of agreement between the observed and expected values, and the best-verified salinity index is SI 7, which has a low estimated RMSE error of 8.58, this result is also similar to [47].

4.5. Model Validation Using Tukey's Test

Tukey's statistical test is a single-step multiple comparison procedure used to obtain means (expected normal values and observed values of EC_e and accepted soil salinity indices) that are significantly different and detect any differences between these means that is greater than the expected standard error (R^2) [39]. According to Table 7, using 30 test soil samples, the obtained results showed that the highest standard error (R^2) was represented by EC_e, and the lowest one is SI 9. According to [49–51], cross-validation was used to find the degree of agreement between the measured and estimated data based on the expected normal values and observed values of EC_e and accepted soil salinity indices and cross-validation was used for all data to evaluate the autocorrelation model trend, the results of this study reveal that the model provided reasonable prediction and calculated statistics diagnose model and its associated parameter values are reasonable in the study area.

5. Conclusions

Soil salinity assessment is considered to be a keystone for better agriculture management practices. Soil salinity indices are a good method to produce soil salinity maps depending on Landsat-8 (OLI) images, RS and GIS techniques that have the best role for salinity spatial distribution in the investigated area. The obtained results represented that all salinity indices have satisfactory correlations between EC_e values for each soil sample site and salinity indices (SI 5 index represents non-significant correlations with R^2 value of 0.2688, while the SI 8 index shows a higher negative significant correlation with EC_e readings with R^2 value of 0.6356) and there was a significant positive correlation at $p < 0.01$ level between soil EC_e and SI 9 index (r = 0.514). There is a non-significant correlation at the $p < 0.05$ level between soil EC_e and (SI 1, SI 2, SI 7, and SI 8) indices (r = 0.495, 0.491, 0.479, 0.492, respectively), and the best salinity index is SI 7, showing a low estimated RMSE error of 8.58. Finally, the highest standard error (R^2) was represented by EC_e (dS m^{-1}), with an R^2 of 0.881, and the lowest one was for SI 9, with an R^2 of 0.428, according to Tukey test analysis. Therefore, the observation and investigation of soil salinity are essential requirements for appropriate natural resource management plans in the future. This study recommended that salinity indices and Landsat-8 images should be used (soil salinity studies) and represent better methods to produce spatial distribution maps. However, they

require further investigative studies of their dependencies and whether they are valid for use in other studies under arid regions with the same conditions, i.e., climate conditions, precipitation, evaporation rate, drainage or waterlogging (a raised water table), irrigation water, vegetation cover, leakage from geological deposits and penetration into groundwater, sea-level rise when sea salts seep into lower lands and inappropriate application of fertilizers when excess nitrification accelerates soil salinization.

Author Contributions: Conceptualization, M.E.F., M.E.M.J., M.A.E.A., W.R.Z., A.S.A., A.A.B. and A.S.; Methodology, M.E.F., M.A.E.A., E.A.A., W.R.Z., A.A.B., P.D. and A.S.; Software, M.E.F., M.A.E.A., A.S.A., C.F. and A.A.B.; Validation, M.E.F., M.E.M.J., M.A.E.A., W.R.Z., A.S.A., A.A.B., P.D. and A.S.; Formal analysis, M.E.F., M.A.E.A., E.A.A., A.S.A., A.A.B., C.F. and A.S.; Investigation, M.E.F., M.A.E.A. and A.S.A.; Resources, M.E.F., M.A.E.A., W.R.Z. and A.S.A.; Data curation, M.E.F., M.E.M.J., M.A.E.A., W.R.Z., A.S.A., A.A.B., P.D., C.F. and A.S.; Writing—original draft preparation, M.E.F., M.E.M.J., M.A.E.A., E.A.A., W.R.Z., A.S.A., A.A.B., P.D., C.F. and A.S.; Writing—review and editing, M.E.F., M.A.E.A., E.A.A., W.R.Z., A.S.A., A.A.B., P.D., C.F. and A.S.; Visualization, M.E.F., M.E.M.J., M.A.E.A., W.R.Z., A.S.A., A.A.B. and A.S.; Supervision, M.E.F. and A.S.; Project administration, M.E.F., M.A.E.A., W.R.Z., A.S.A., A.A.B. and A.S.; Funding acquisition A.S. and P.D. All authors have read and agreed to the published version of the manuscript.

Institutional Review Board Statement: Not applicable.

Informed Consent Statement: Not applicable.

Data Availability Statement: Not applicable.

Conflicts of Interest: The authors would like to hereby certify that there are no conflicts of interest in the data collection, analyses, and interpretation, in the writing of the manuscript, and in the decision to publish the results. The authors would also like to declare that the funding of the study has been supported by the authors' institutions.

References

1. Gorji, T.; Sertel, E.; Tanik, A. Monitoring soil salinity via remote sensing technology under data scarce conditions: A case study from Turkey. *Ecol. Indic.* **2017**, *74*, 384–391. [CrossRef]
2. Gorji, T.; Yildirim, A.; Hamzehpour, N.; Tanik, A.; Sertel, E. Soil salinity analysis of Urmia Lake Basin using Landsat-8 OLI and Sentinel-2A based spectral indices and electrical conductivity measurements. *Ecol. Indic.* **2020**, *112*, 106173. [CrossRef]
3. Song, C.; Ren, H.; Huang, C. Estimating Soil Salinity in the Yellow River Delta, Eastern China—An Integrated Approach Using Spectral and Terrain Indices with the Generalized Additive Model. *Pedosphere* **2016**, *26*, 626–635. [CrossRef]
4. Elhag, M.; Bahrawi, J.A. Soil salinity mapping and hydrological drought indices assessment in arid environments based on remote sensing techniques. *Geosci. Instrum. Methods Data Syst.* **2017**, *6*, 149–158. [CrossRef]
5. Metternicht, G.I.; Zinck, J.A. Remote sensing of soil salinity: Potentials and constraints. *Remote Sens. Environ.* **2003**, *85*, 1–20. [CrossRef]
6. Dwivedi, R.S. Soil resources mapping: A remote sensing perspective. *Remote Sens. Rev.* **2001**, *20*, 89–122. [CrossRef]
7. Allbed, A.; Kumar, L. Soil salinity mapping and monitoring in arid and semi-arid regions using remote sensing technology: A review. *Adv. Remote Sens.* **2013**, *2*, 373–385. [CrossRef]
8. Mohamed, E.S.; Belal, A.; Saleh, A. Assessment of land degradation east of the Nile Delta, Egypt using remote sensing and GIS techniques. *Arab. J. Geosci.* **2012**, *6*, 2843–2853. [CrossRef]
9. Behera, S.K.; Shukla, A.K. Spatial distribution of surface soil acidity, electrical conductivity, soil organic carbon content and exchangeable potassium, calcium and magnesium in some cropped acid soils of India. *Land Degrad. Dev.* **2015**, *26*, 71–79. [CrossRef]
10. Saleh, A.M.; Belal, A.B.; Mohamed, E.S. Land resources assessment of El-Galaba basin, South Egypt for the potentiality of agriculture expansion using remote sensing and GIS techniques. *Egypt. J. Remote Sens. Space Sci.* **2015**, *18*, S19–S30. [CrossRef]

11. Saleh, A.M.; Belal, A.B.; Mohamed, E.S. Mapping of Soil Salinity Using Electromagnetic Induction: A Case Study of East Nile Delta, Egypt. *Egypt. J. Soil Sci.* **2017**, *57*, 167–174. [CrossRef]

12. Abuzaid, A.S.; Abdellatif, A.D.; Fadl, M.E. Modeling soil quality in Dakahlia Governorate, Egypt using GIS techniques. *Egypt. J. Remote Sens. Space Sci.* **2021**, *24*, 255–264. [CrossRef]

13. Jiapaer, G.; Chen, X.; Bao, A. A comparison of methods for estimating fractional vegetation cover in arid regions. *Agric. For. Meteorol.* **2011**, *151*, 1698–1710. [CrossRef]

14. Soriano-Disla, J.M.; Janik, L.S.; Viscara Rossel, R.A.; Macdonald, L.M.; McLaughlin, M.J. The Performance of Visible, Near-, and Mid-Infrared Reflectance Spectroscopy for Prediction of Soil Physical, Chemical, and Biological Properties. *Appl. Spectrosc. Rev.* **2014**, *49*, 139–186. [CrossRef]

15. Abuzaid, A.S.; AbdelRahman, M.A.E.; Fadl, M.E.; Scopa, A. Land Degradation Vulnerability Mapping in a Newly-Reclaimed Desert Oasis in a Hyper-Arid Agro-Ecosystem Using AHP and Geospatial Techniques. *Agronomy* **2021**, *11*, 1426. [CrossRef]

16. Selmy, S.A.H.; Abd Al-Aziz, S.H.; Jiménez-Ballesta, R.; García-Navarro, F.J.; Fadl, M.E. Modeling and Assessing Potential Soil Erosion Hazards Using USLE and Wind Erosion Models in Integration with GIS Techniques Dakhla Oasis, Egypt. *Agriculture* **2021**, *11*, 1124. [CrossRef]

17. Fadl, M.E.; Abuzaid, A.S.; AbdelRahman, M.A.E.; Biswas, A. Evaluation of Desertification Severity in El-Farafra Oasis, Western Desert of Egypt: Application of Modified MEDALUS Approach Using Wind Erosion Index and Factor Analysis. *Land* **2022**, *11*, 54. [CrossRef]

18. Bartholomeus, K.L.; Antoine, S.; Martin, V.L.; Bas, V.W.; Ben-Dor, E.; Bernard, T. Soil organic carbon mapping of partially vegetated agricultural fields with imaging spectroscopy harm. *Int. J. Appl. Earth Obs. Geoinf.* **2011**, *13*, 81–88. [CrossRef]

19. Stevens, A.; van-Wesemael, B.; Bartholomeus, H.; Tychon, B.; Ben-Dor, E. Laboratory, field and airborne spectroscopy for monitoring organic carbon content in agricultural soils. *Geoderma* **2008**, *144*, 395–404. [CrossRef]

20. Weng, Y.; Gong, P.; Zhu, Z.-L. Soil sail content estimation in the Yellow River delta with satellite hyperspectral data. *Can. J. Remote Sens.* **2008**, *34*, 259–270.

21. Ogen, Y.; Zaludab, J.; Francosb, N.; Goldshlegerc, N.; Ben-Dor, E. Cluster-based spectral models for a robust assessment of soil properties. *Geoderma* **2019**, *340*, 175–184. [CrossRef]

22. Wold, S.; Sjöström, M.; Eriksson, L. PLS-regression: A basic tool of chemometrics. *Chemom. Intell. Lab. Syst.* **2001**, *58*, 109–130. [CrossRef]

23. Woodcock, C.E. Uncertainty in remote sensing. In *Uncertainty in Remote Sensing and GIS*; Atkinson, P.M., Foody, G.M., Eds.; John Wiley & Sons: Hoboken, NJ, USA, 2003; pp. 19–24. ISBN 0-470-84408-6.

24. National Oceanic and Atmospheric Administration (NOAA). El-Farafra Climate Normals"Appendix I: Meteorological Data". 2020. Available online: https://www.noaa.gov/ (accessed on 11 February 2022).

25. Soil Survey Staff. *Keys to Soil Taxonomy*, 12th ed.; United States Department of Agriculture, Natural Resources Conservation Service: Washington, DC, USA, 2014; pp. 1–372.

26. ENVI. *ENVI User's Guide. Software Package ver. 5.3.*; Research Systems Inc.: Boulder, CO, USA, 2018; p. 1128.

27. *Esri Arc Map, version 10.2.2*; Esri: Redlands, CA, USA, 2014.

28. Soil Survey Staff. *Soil Survey Laboratory Methods Manual. Soil Survey Investigations: Report 42, Version 4.0*; United States Department of Agriculture, Natural Resources Conservation Service, National Soil Survey Center: Lincoln, NE, USA, 2004.

29. Bashour, I.I.; Sayegh, A.H. *Methods of Analysis for Soils of Arid and Semi-Arid Regions*; FAO: Rome, Italy, 2007.

30. Soil Survey Staff. *Soil Survey Field and Laboratory Methods Manual: Soil Survey Investigations Report No. 51, Version 2.0*; U.S. Department of Agriculture, Natural Resources Conservation Service: Washington, DC, USA, 2014; pp. 1–488.

31. U.S. Salinity Laboratory Staff. *Diagnosis and Improvement of Saline and Alkali Soils*; Richards, L.A., Ed.; United States Department of Agriculture: Washington, DC, USA, 1954; Volume 60, pp. 1–166.

32. Khan, N.M.; Rastoskuev, V.V.; Sato, Y.; Shiozawa, S. Assessment of hydrosaline land degradation by using a simple approach of remote sensing indicators. *Agric. Water Manag.* **2005**, *77*, 96–109. [CrossRef]

33. Bannari, A.; Guedon, A.; El-Harti, A.; Cherkaoui, F.; El-Ghmari, A. Characterization of slightly and moderately saline and sodic soils in irrigated agricultural land using simulated data of advanced land imaging (EO-1) sensor. *Commun. Soil Sci. Plant Anal.* **2008**, *39*, 2795–2811. [CrossRef]

34. Abbas, A.; Khan, S. Using Remote Sensing Techniques for Appraisal of Irrigated Soil Salinity. In *International Congress on Modelling and Simulation (MODSIM)*; Oxley, L., Kulasiri, D., Eds.; Modelling and Simulation Society of Australia and New Zealand: Brighton, UK, 2007; pp. 2632–2638.

35. Liu, Y.; Harding, A.; Gilbert, R.; Journal, A.G. A Workflow for Multiple-point Geostatistical Simulation. In *Geostatistics Banff 2004*; Leuangthong, O., Deutsch, C.V., Eds.; Springer: Dordrecht, The Netherlands, 2005; pp. 245–254.

36. Jain, P.; Ramsankaran, R. GIS-based modelling of soil erosion processes using the modified-MMF (MMMF) model in a large watershed having vast agro-climatological differences. *Earth Surf. Process. Landf.* **2018**, *43*, 2064–2076. [CrossRef]

37. Cohen, J. *Statistical Power Analysis for the Behavioral Sciences*, 2nd ed.; Routledge: New York, NY, USA, 1988. [CrossRef]

38. Barnston, A.G. Correspondence among the correlation, RMSE, and Heidke forecast verification measures; refinement of the Heidke score. *Weather. Forecast.* **1992**, *7*, 699–709. [CrossRef]

39. Tukey, J. Comparing individual means in the analysis of variance. *Biometrics* **1949**, *5*, 99–114. [CrossRef]

40. Linton, L.; Harder, L. *Biology 315–Quantitative Biology Lecture Notes*; University of Calgary: Calgary, AB, Canada, 2007.

41. Beek, K.J.; Blokhuis, W.A.; Driessen, P.M.; Van Breemen, N.; Brinkman, R.; Pons, L.J. Problem soils: Their reclamation and management. In *Land Reclamation and Water Management, Developments, Problems and Challenges*; International Institute for Land Reclamation and Improvement (ILRI): Wageningen, The Netherlands, 1980; pp. 43–72.

42. Nawar, S.; Buddenbaum, H.; Hill, J.; Kozak, J. Modeling and mapping of soil salinity with reflectance spectroscopy and Landsat data using two quantitative methods (PLSR and MARS). *Remote Sens.* **2014**, *6*, 10813–10834. [CrossRef]

43. Farifteh, J.; Van der Meer, F.; Atzberger, C.; Carranza, E. Quantitative analysis of salt-affected soil reflectance spectra: A comparison of two adaptive methods (PLSR and ANN). *Remote Sens. Environ.* **2007**, *110*, 59–78. [CrossRef]

44. Yan, X.; Su, X. *Linear Regression Analysis: Theory and Computing*; World Scientific: Hackensack, NJ, USA, 2009; p. 328.

45. Zhang, T.-T.; Qi, J.-G.; Gao, Y.; Ouyang, Z.-T.; Zeng, S.-L.; Zhao, B. Detecting soil salinity with MODIS time series VI data. *Ecol. Indic.* **2015**, *52*, 480–489. [CrossRef]

46. Sidike, A.; Zhao, S.; Wen, Y. Estimating soil salinity in Pingluo County of China using QuickBird data and soil reflectance spectra. *Int. J. Appl. Earth Obs. Geoinf.* **2014**, *26*, 156–175. [CrossRef]

47. Hammam, A.; Mohamed, E. Mapping soil salinity in the East Nile Delta using several methodological approaches of salinity assessment. *Egypt. J. Remote Sens. Space Sci.* **2020**, *23*, 125–131. [CrossRef]

48. Kenney, J.F.; Keeping, E. Linear regression and correlation. *Math. Stat.* **1962**, *1*, 252–285.

49. Zaidelman, F.R. Deep reclamation loosening of soils: State of the problem, results of research, prospects of application, and degradation changes. *Eurasian Soil Sc.* **2016**, *49*, 1061–1074. [CrossRef]

50. Erkin, N.; Zhu, L.; Gu, H.; Tusiyiti, A. Method for predicting soil salinity concentrations in croplands based on machine learning and remote sensing techniques. *J. Appl. Remote Sens.* **2019**, *13*, 034520. [CrossRef]

51. Fourati, H.T.; Bouaziz, M.; Benzina, M.; Bouaziz, S. Detection of terrain indices related to soil salinity and mapping salt-affected soils using remote sensing and geostatistical techniques. *Environ. Monit. Assess.* **2017**, *189*, 177. [CrossRef]